Hindawi
International Journal of Antennas and Propagation
Volume 2024, Article ID 6640727, 9 pages
https://doi.org/10.1155/2024/6640727

Research Article

Evaluation of the Inductive Coupling between Coplanar Concentric Coils in the Presence of the Ground

Mauro Parise

Department of Engineering, University Campus Bio-Medico of Rome, Via Alvaro del Portillo 21, Rome 00128, Italy

Correspondence should be addressed to Mauro Parise; m.parise@unicampus.it

Received 19 June 2023; Revised 13 July 2023; Accepted 23 February 2024; Published 8 March 2024

Academic Editor: Rajkishor Kumar

An analytical approach is presented that allows deriving an exact series-form representation for the flux linkage between two physically large concentric circular coils located on a lossy soil. The expression comes from a three-step analytical procedure. First, the integral expression for the flux linkage is converted into a double integral consisting of a finite and a semi-infinite integral. Next, the semi-infinite integral is recognized to be a well-known tabulated Sommerfeld integral, which may be analytically evaluated straightforwardly. Finally, applying Lommel's expansion allows rewriting the remaining finite integral as a sum of elementary integrals amenable to analytical evaluation. As a result, the flux linkage between the two coils is given as a sum of spherical Hankel functions of the wavenumber in the air and in the ground, multiplied by a coefficient depending on the geometrical dimensions of the coils. The accuracy and robustness of the proposed formulation is tested by comparing its outcomes with those generated by numerical integration of the complete integral representation for the flux linkage and with the results provided by previous analytical approaches to the same problem. It is found that the use of the derived expression for the inductance makes it possible to obtain significant time savings as compared to numerical quadrature schemes.

1. Introduction

In recent years, current-carrying coils of wire have been extensively used in a number of fields of scientific and technological interest, including electromagnetic sounding for earth exploration [1, 2], magnetic resonance imaging [3–5], radio direction finding [6–9], diathermy [10, 11], and wireless power transfer (WPT) [12]. In several engineering applications, coil antennas are arranged in pairs or organized within an array structure, with the scope of transmitting electric power, measuring the direction of arrival of a radio signal, or acquiring information about the subsurface structure of a terrestrial area and detecting shallow buried objects. For instance, with the growing demand for battery electric vehicles (BEVs), two-coil WPT systems capable of efficient energy transfer are increasingly requested. Basically, WPT systems for battery electric vehicles are used to transfer electrical energy from a source coil to a receiving coil connected to a charging system. The peculiarity of this process lies in the fact that the energy transfer is performed via magnetic induction, without wires and cables [13–17]. It turns out that the magnetic coupling between the coils plays a fundamental role in the efficiency of the energy transfer, and the determination of the mutual inductance between the emitter and the receiver becomes necessary to get helpful knowledge about the coupling strength.

In literature, many works have addressed the problem of rigorously calculating the mutual inductance in a free-space environment [18–27]. Unfortunately, such solutions cannot be used every time that the coils are located in close proximity to or on the top surface of a terrestrial area, which happens, for instance, in applications like WPT systems for BEV, where the coils operate close to the bottom part of the vehicle. Here, the presence of the soil has a considerable impact on the mutual coupling and, hence, on the performance of the energy transfer.

Despite the importance of evaluating the flux linkage between coaxial coils located in proximity to terrestrial areas, there is scarcity of analytical solutions that allow accomplishing this task. An attempt in this direction has been

made in [28], where the problem of two coils placed at the air-ground interface is considered. Unfortunately, the derived solution for the mutual impedance is valid only for equally sized coils separated by a non-negligible radial distance and when taking the limit as the distance approaches zero (that is, when the coils share the same axis), the obtained formula diverges. To author's knowledge, the sole analytical approaches that efficiently treat this problem are the well-established quasistatic explicit expression for the inductance [29] or the improved analytical solution derived in [30], valid in a wider frequency range. Yet, both these solutions have the disadvantage of being subject to the condition that the receiving coil is physically and electrically small (small-loop assumption) and, as a consequence, they cannot be used for arbitrarily sized coils.

Thus, the computation of the mutual inductance of coaxial coils located above an earth structure is usually carried out by using three-dimensional simulation techniques such as the boundary element method (BEM) and the finite element method (FEM) or via numerical integration of its integral expression. However, especially if the coil system is supposed to operate very close to or on the top surface of the ground, these methods involve significant computational efforts, which, in turn, imply non-negligible time costs.

The scope of the present work is to derive an exact explicit expression for the flux linkage between two physically large concentric circular coils positioned on the top surface of a homogeneous material medium, which responds to the following two requirements. First, it must be valid in the quasistatic as well as nonquasistatic frequency regions and regardless of the coils size. Second, it must exhibit advantages in terms of time cost with respect to numerical techniques. Starting from the infinite integral representation for the flux linkage, the expression is obtained by converting the product of the two Bessel functions contained in the integrand into the finite integral of one Bessel function. Then, the infinite and the finite integral signs are interchanged, and the infinite integration is recognized to be a well-known tabulated Sommerfeld integral, whose analytical evaluation is straightforward. Finally, applying Lommel's expansion permits to turn the remaining finite integral into a sum of simpler integrals amenable to analytical evaluation. As a result of the developed theory, the mutual inductance is expressed as a sum of spherical Hankel functions of the wavenumber in the air and in the conducting medium, multiplied by a coefficient depending on geometrical parameters. The derived formula holds under the thin-wire assumption, which prescribes that the radii of the coils must be far greater than the wire radius. The validity of the proposed approach is tested through comparison with the data provided by numerical integration of the integral representation for the mutual inductance, as well as with the outcomes from the previously published quasistatic solution to the same problem. What emerges is that the derived exact expression for the inductance is advantageous over numerical quadrature schemes as, accuracy being equal, its usage ensures considerable time savings with respect to numerical integration. On the other hand, the proposed expression allows relaxing the quasistatic assumption and the hypothesis of small receiving coil, both underlying the previous solution to the problem.

2. Theory

The geometric configuration of the problem is shown in Figure 1. Two concentric large circular loops, with radii a and $(a > b)$, are placed on the surface of a homogeneous medium. The wire that constitutes each coil is assumed to be thin, which implies that the wire radius r_0 is much smaller than the external radius of the coil ($r_0 \ll a, b$). The magnetic permeability is taken to be everywhere that of free space μ_0, while the dielectric constant and electric conductivity of the material medium are denoted by ϵ_1 and σ_1, respectively.

Our scope is to determine an exact explicit expression for the mutual inductance M of the two loops, which is not subject to any restrictive assumption. This will be done by introducing an efficient method that allows to evaluate the integral representation for M. If, for the purposes of the derivation, the primary coil is taken to be the larger loop of Figure 1, the mutual inductance is defined as the flux encompassed by the receiving coil per unit current flowing in the source coil. Thus, after setting $I = 1$ A, with the time factor $e^{j\omega t}$ assumed and suppressed for notational simplicity, it reads

$$M = \mu_0 \int_0^b \int_0^{2\pi} H_z(r) r \, \mathrm{d}r \, \mathrm{d}\vartheta, \tag{1}$$

where r and ϑ are, as depicted in Figure 1(b), the polar coordinates of the generic field point, while H_z is the vertical magnetic field generated by the source loop, given by [[29], 4.88]

$$H_z(r) = a \int_0^\infty \frac{1}{u_0 + u_1} J_1(k_\rho a) J_0(k_\rho r) k_\rho^2 \, \mathrm{d}k_\rho, \tag{2}$$

with $J_\nu(\cdot)$ being the ν th-order Bessel function, and with

$$\begin{aligned} u_n &= \sqrt{k_\rho^2 - k_n^2}, \ \mathrm{Re}[u_n] > 0, \\ k_n^2 &= \omega^2 \mu_n \epsilon_n - j\omega \mu_n \sigma_n, \end{aligned} \tag{3}$$

where $\sigma_0 = 0$ and $\mu_1 = \mu_0$. The use of (2) into (1) provides the following expression for M:

$$\begin{aligned} M &= \mu_0 a \int_0^\infty \frac{k_\rho^2}{u_0 + u_1} J_1(k_\rho a) \left[\int_0^b \int_0^{2\pi} J_0(k_\rho r) \, r \, \mathrm{d}r \, \mathrm{d}\vartheta \right] \mathrm{d}k_\rho \\ &= 2\pi \mu_0 a \int_0^\infty \frac{k_\rho^2}{u_0 + u_1} J_1(k_\rho a) \left[\int_0^b J_0(k_\rho r) \, r \, \mathrm{d}r \right] dk_\rho, \end{aligned} \tag{4}$$

and after introducing the well-known identity [[31], 5.52.1],

$$\int_0^b J_0(k_\rho r) r \, \mathrm{d}r = \frac{b}{k_\rho} J_1(k_\rho b), \tag{5}$$

and expression (4) is turned into

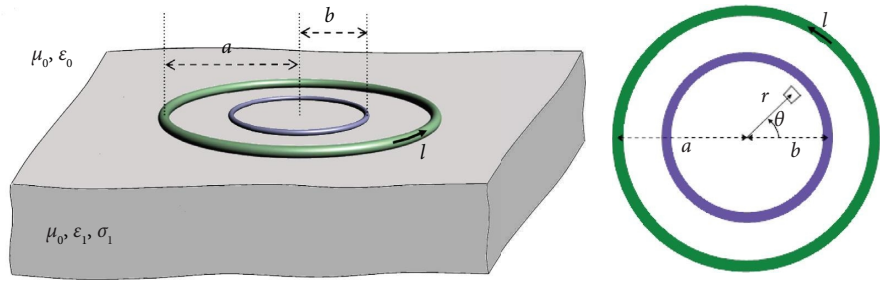

(a) (b)

FIGURE 1: (a) Isometric and (b) top views of the geometry under study.

$$M = 2\pi\mu_0 ab \int_0^{\infty} \frac{1}{u_0 + u_1} J_1\left(k_\rho a\right) J_1\left(k_\rho b\right) k_\rho \mathrm{d}k_\rho, \tag{6}$$

which is the exact integral representation for the flux linkage between the coils. Since it holds [[32], 11.41.17]

$$J_m(\alpha)\, J_m(\beta) = \frac{1}{\pi} \int_0^{\pi} J_0(\gamma) \cos m\vartheta \, \mathrm{d}\vartheta, \tag{7}$$

with

$$\gamma = \sqrt{\alpha^2 + \beta^2 - 2\alpha\beta\cos\vartheta}, \tag{8}$$

formula (6) may be expressed as

$$M = 2\mu_0 ab \int_0^{\pi} \cos\vartheta \, \mathrm{d}\vartheta \int_0^{\infty} \frac{1}{u_0 + u_1} J_0\left(k_\rho R\right) k_\rho \, \mathrm{d}k_\rho, \tag{9}$$

with $R = \sqrt{a^2 + b^2 - 2ab\cos\vartheta}$. The semi-infinite integral in (9) may be evaluated by multiplying the numerator and denominator of the integrand by $u_0 - u_1$ and then making use of the identity [33]

$$u_n^2 J_0\left(k_\rho R\right) = -\left(\nabla_t^2 + k_n^2\right) J_0\left(k_\rho R\right), \tag{10}$$

with

$$\nabla_t^2 = \frac{1}{R} \frac{\partial}{\partial R} \left(R \frac{\partial}{\partial R} \right). \tag{11}$$

It yields

$$\begin{aligned} \int_0^{\infty} \frac{1}{u_0 + u_1} J_0\left(k_\rho R\right) k_\rho \mathrm{d}k_\rho &= \frac{1}{k_1^2 - k_0^2} \int_0^{\infty} (u_0 - u_1) J_0\left(k_\rho R\right) k_\rho \mathrm{d}k_\rho \\ &= \frac{1}{k_1^2 - k_0^2} \left\{ \int_0^{\infty} \frac{u_n^2}{u_n} J_0\left(k_\rho R\right) k_\rho \mathrm{d}k_\rho \right\}_{n=1}^{n=0} \\ &= -\frac{1}{k_1^2 - k_0^2} \left\{ \left(\nabla_t^2 + k_n^2\right) \int_0^{\infty} \frac{1}{u_n} J_0\left(k_\rho R\right) k_\rho d k_\rho \right\}_{n=1}^{n=0}, \end{aligned} \tag{12}$$

where the integral on the right-hand side is well-known and given by [[34], p. 677, no. 13]

$$\int_0^{\infty} \frac{1}{u_n} J_0\left(k_\rho R\right) k_\rho \mathrm{d}k_\rho = -jk_n h_0^{(2)}(k_n R), \tag{13}$$

with $h_0^{(2)}(\xi)$ being the zeroth-order spherical Hankel function of the second kind. The use of (12) together with (13) into (9) provides

$$M = \frac{2j\mu_0 ab}{k_1^2 - k_0^2} \left\{ k_n \int_0^{\pi} \left(\nabla_t^2 + k_n^2\right) \left[h_0^{(2)}(k_n R) \right] \cos\vartheta \, \mathrm{d}\vartheta \right\}_{n=1}^{n=0}, \tag{14}$$

and since it is not difficult to prove that

$$\left(\nabla_t^2 + k_n^2\right) \left[h_0^{(2)}(k_n R) \right] = \frac{k_n}{R} h_1^{(2)}(k_n R), \tag{15}$$

one obtains

$$M = \frac{2j\mu_0 ab}{k_1^2 - k_0^2} \left[k_n^3 \int_0^{\pi} g_1(k_n R) \cos\vartheta \, \mathrm{d}\vartheta \right]_{n=1}^{n=0}, \tag{16}$$

where it has been set

$$g_l(\xi) = \frac{h_l^{(2)}(\xi)}{\xi^l}. \tag{17}$$

The finite integral may be analytically evaluated once g_1 is replaced with its Maclaurin expansion with respect to $\cos\vartheta$. If we let $\tau = -2ab\cos\vartheta$, the expansion is given by

$$g_l(k_nR) = \sum_{m=0}^{\infty} \frac{\tau^m}{m!} \left[\frac{d^m g_l(k_nR)}{d\tau^m} \right]_{\tau=0}, \tag{18}$$

and since from the differentiation properties of the spherical Bessel functions [[33], 10.1.24], it is easily deduced that

$$\frac{d}{d\xi}[g_l(\xi)] = -\xi\, g_{l+1}(\xi), \tag{19}$$

one obtains the relation

$$\frac{d}{d\tau}[g_l(k_nR)] = \left(-\frac{k_n^2}{2}\right) g_{l+1}(k_nR), \tag{20}$$

which may be applied recursively to give

$$\frac{d^m}{d\tau^m}[g_l(k_nR)] = \left(-\frac{k_n^2}{2}\right)^m g_{l+m}(k_nR). \tag{21}$$

The use of (21) into (18) provides

$$g_l(k_nR) = \sum_{m=0}^{\infty} \frac{1}{m!} \left(-\frac{k_n^2\tau}{2}\right)^m g_{l+m}\left(k_n\sqrt{a^2+b^2}\right), \tag{22}$$

and for $l = 1$, the following expansion is found:

$$g_1(k_nR) = \sum_{m=0}^{\infty} \frac{1}{m!} \left(-\frac{k_n^2\tau}{2}\right)^m g_{m+1}\left(k_n\sqrt{a^2+b^2}\right), \tag{23}$$

which, substituted for g_1 in (16), leads to

$$M = \frac{2j\mu_0}{k_1^2 - k_0^2} \sum_{m=0}^{\infty} \frac{1}{m!} \left[k_n \left(k_n^2 ab\right)^{m+1} g_{m+1}\left(k_n\sqrt{a^2+b^2}\right) \right]_{n=1}^{n=0} \int_0^{\pi} \cos^{m+1}\vartheta\, d\vartheta. \tag{24}$$

The integral on the right-hand side is tabulated and given by [[31], 2.512.2–2.512.3]

$$\int_0^{\pi} \cos^{m+1}\vartheta\, d\vartheta = \begin{cases} 0, & \text{even } m, \\ \pi\, m!!/(m+1)!!, & \text{odd } m, \end{cases} \tag{25}$$

where $m!!$ denotes the double factorial. Thus, after setting $m = 2l - 1$, expression (24) becomes

$$M(a, b) = \frac{2\pi j\mu_0}{k_1^2 - k_0^2} \sum_{l=1}^{\infty} \frac{1}{(2l)!![2(l-1)]!!} \left[k_n (k_n r)^{2l} h_{2l}^{(2)}\left(k_n\sqrt{a^2+b^2}\right) \right]_{n=1}^{n=0}, \tag{26}$$

where account has been taken that $(2l-1)! = (2l-1)!!\,(2l-2)!!$, and with

$$r = \frac{ab}{\sqrt{a^2+b^2}}, \tag{27}$$

and [35]

$$h_m^{(2)}(\xi) = j^{m+1} \frac{e^{-j\xi}}{\xi} \sum_{i=0}^{m} \frac{(m+i)!}{i!\,(m-i)!} (2j\xi)^{-i}. \tag{28}$$

It should be noted that the obtained representation (26) for the flux linkage may be also used to obtain the self-loop inductance of each coil. In fact, for a loop with external radius a and wire radius r_w, the self-inductance under the thin-wire assumption (that is, $r_w \ll a$) is given by

$$L(a, r_w) = M(a, a - r_w). \tag{29}$$

Finally, the expression for the mutual inductance of a pair of circular loops may be applied to the computation of the flux linkage between multiturn coils. If, as an example, the emitter is a single-turn coil with radius a, while the receiver is a pancake coil composed of N_b turns, with radii denoted by $b_i\,(i = 1, 2, \ldots, N_b)$, the mutual inductance between them reads [26]

$$M_{\text{tot}} = \sum_{i=1}^{N_b} M(a, b_i), \tag{30}$$

while the overall self-inductance of the receiver is given by

$$L_{\text{tot}} = \sum_{i=1}^{N_b} L(b_i, r_w) + 2\sum_{i=1}^{N_b} \sum_{l=i+1}^{N_b} M(b_i, b_l). \tag{31}$$

It should be observed that (26) may be used provided that the source loop supports a uniform current. In fact, expression (2), underlying the proposed approach, is based on the uniform current assumption which, in principle, holds if the length of the wire that constitutes the source loop is less than or equal to 0.3 times the free-space wavelength λ [36]. For electrically larger antennas, the variations of the current along the loop become large and (2) cannot be used any longer, unless a uniform current is forced by the feeding system. As explained in [37, 38], this may be done by dividing the source coil into electrically short segments and then by driving them in parallel by means of radial transmission lines.

3. Results and Discussion

The validity and robustness of the proposed approach is tested by applying the derived expression (26) to the computation of the flux linkage between two coaxial coils

placed on a clay soil. The electrical conductivity and dielectric permittivity of the soil are taken to be equal to $\sigma_1 = \sigma = 10\,\text{mS/m}$ and $\epsilon_1 = 10\,\epsilon_0$, respectively [39]. At first, the real and imaginary parts of M are computed against the operating frequency, with $b = 0.5$ m and $a = 5$ m. The obtained results, illustrated in Figure 2, are compared with the data provided by both numerical integration of (6) and the finite difference time domain (FDTD) method. In particular, numerical integration is carried out by using an adaptive Gauss–Kronrod G7-K15 scheme, arising from the combination of a 7-point Gauss rule with a 15-point Kronrod rule. On the other hand, the FDTD lattice is configured with $300 \times 300 \times 20$ cubic cells with side lengths of 5 cm, spanning a computational domain of $15 \times 15 \times 1$ m enclosing the coils. The mesh is terminated with PML absorbing boundary conditions in the three Cartesian directions.

In addition, for the sake of comparison, the results are also compared with those obtained by using the quasistatic approximation for the produced magnetic field, derived under the further assumption that the receiver is both electrically and physically small. In this situation, the mutual inductance is simply given by the vertical magnetic field H_z^0 generated by the emitter at its center, multiplied by the magnetic permeability in free space and the area of the receiving coil. It reads $M = \mu_0 \pi b^2 H_z^0$, where the quasistatic approximation for H_z^0 is given by [29]

$$H_z^0 = -\frac{1}{k_1^2 a^3}\left[3 - \left(3 + 3jk_1 a - k_1^2 a^2\right) e^{-jk_1 a}\right]. \tag{32}$$

As is shown by Figure 2, the curves arising from (26) approach the data originating from the numerical integration of the complete representation (6) as L is increased, with L being the index of truncation of the sum in (26). In particular, excellent agreement is observed for $L = 3$ all over the considered frequency range, which implies that these trends may be referred to as exact curves. Conversely, the profiles of the real and imaginary parts of M arising from the quasistatic solution (32) are in agreement with the respective exact curves only in the low-frequency range, up to about 10 MHz (real part of M) and 3 MHz (imaginary part of M). These frequency limits are consistent with the theoretical upper limit of validity of the quasistatic assumption. To convince on this point, it suffices to consider that the quasistatic assumption is valid as long as the largest dimension D of the considered system is electrically small, that is, for $\lambda \gg D$, with λ being the free-space wavelength. This ensures that the overall size of the two-loop system is sufficiently small for electromagnetic retardation to have negligible impact on the field distribution. Since, in the present configuration, D coincides with the diagonal of the square bounding box enclosing the loops, which is $2a\sqrt{2}$ long, the quasistatic field assumption implies that

$$\lambda \geq 10D = 20a\sqrt{2}, \tag{33}$$

and, as a consequence, it holds as long as the operating frequency f obeys the inequality

$$f \leq f_{\max} = \frac{c}{20a\sqrt{2}} = \frac{3 \cdot 10^8}{10^2\sqrt{2}} \cong 2.12\,\text{MHz}, \tag{34}$$

with c being the speed of light in vacuum. Thus, $f_{\max}$ is the frequency below which (32) must provide exact results, and this is confirmed by the curves plotted in Figure 1. Thereinafter, the profiles of the real and the imaginary parts of (32) will deviate from the corresponding exact curves, and this may happen at about $f_{\max}$, as in the case of the trend of the imaginary part, or at a higher frequency.

While (26) and numerical integration schemes have been shown to be comparable to each other as far as the exhibited accuracy is concerned, the same cannot be said when it comes to computation time. In fact, the proposed formulation allows achieving significant time savings with respect to purely numerical procedures. This aspect is clarified by Table 1, which shows the average CPU time taken by the proposed approach and Gaussian integration to calculate the profiles depicted in Figure 2. The entries of Table 1 tell us that the speedup offered by (26) is equal to about 376 when $L = 3$, that is, when the curves arising from the two methods coincide. This confirms that the proposed method is significantly faster than Gaussian integration.

On the other hand, investigation of the time cost of (32) would not be useful since this expression cannot provide the same accurate results as the other two methods. In particular, the loss of accuracy of (32) as frequency is increased may be further analyzed by taking a glance at Figure 3, which depicts the relative errors resulting from calculating the real and imaginary parts of M by using (32) instead of numerical integration of (6). From the analysis of the curves plotted in Figure 3(a), it is clearly seen that the relative error of the real part of (32) is less than 1% at frequencies smaller than 1 MHz and is equal to 2% at 3 MHz. Thereinafter, the error rapidly increases as frequency grows up, and beyond 10 MHz, it ranges from 10% to 100% and over. Similar conclusions may be deduced from the analysis of the results depicted in Figure 3(b). Here, the error generated by the imaginary part of (32) is slightly smaller than 0.2% up to 1 MHz. Beyond that frequency, it rapidly grows up, and at 10 MHz, it exceeds 10%.

Additional information on the limitations implied by (32) may be acquired from the investigation of the behavior of the flux linkage between the coils as the radius b of the receiver is changed. This point is illustrated in Figure 4, which depicts the trends of the real and imaginary parts of the mutual inductance against b, calculated by using the same methods as in the previous example. The radius of the emitter and the ground conductivity are taken to be $a = 5$ m and $\sigma_1 = 10$ mS/m, respectively, while the operating frequency is assumed to be $f = 10$ MHz. The received radius is assumed to span the $0.05\,m \leq b \leq 2$ m interval. On one hand, the trends shown in Figure 4 confirm that the data provided by (26) converge to the exact results as L is increased. On the other hand, the plotted data clearly point out that the small-loop approximation (32) cannot entirely capture the exact

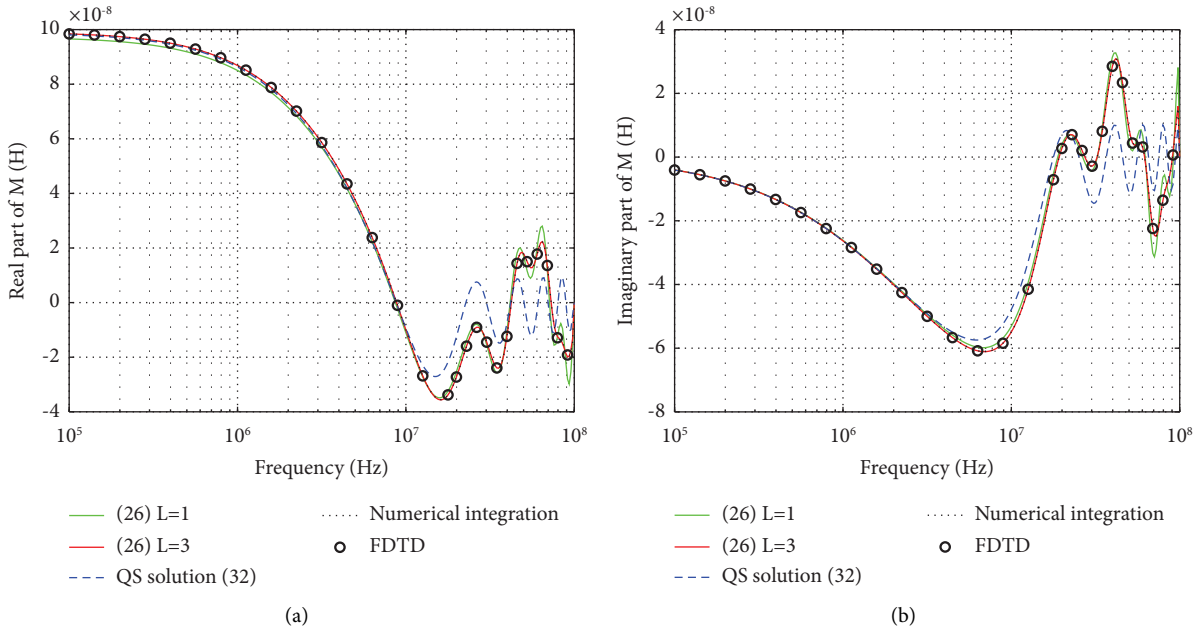

Figure 2: Frequency spectra of the flux linkage between two coils placed on a conducting soil. (a) Frequency spectrum of the real part of the flux linkage. (b) Frequency spectrum of the imaginary part of the flux linkage.

Table 1: CPU time comparisons for the calculation of M against frequency.

Approaches	Average CPU time (s)	Speedup
Gaussian integration	0.05	—
(26) with $L = 1$	$6.64 \cdot 10^{-5}$	753.01
(26) with $L = 2$	$1.04 \cdot 10^{-4}$	480.8
(26) with $L = 3$	$1.33 \cdot 10^{-4}$	375.9

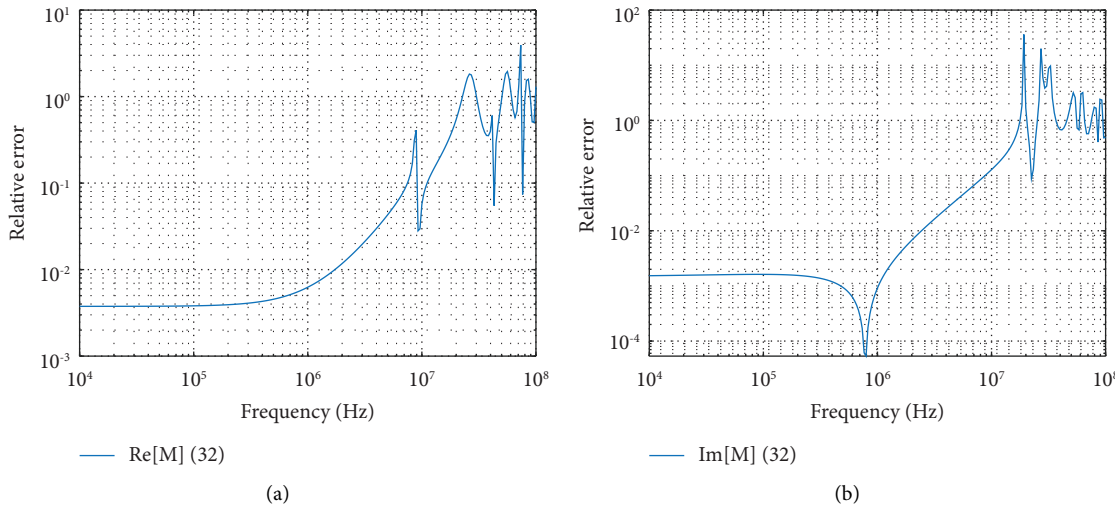

Figure 3: Relative errors of the real and imaginary parts of (32) as compared to the numerical integration of (6) plotted against the operating frequency. (a) Relative error of the real part of (32) against frequency. (b) Relative error of the imaginary part of (32) against frequency.

trend of the inductance, and that, in particular, it fails as soon as b becomes large enough to be comparable to the radius of the emitter. In fact, at the frequency of 10 MHz, the receiver ceases to be physically small well before its size becomes comparable to the free-space wavelength, which event occurs when the length of the wire constituting the receiver, that is, $2\pi b$, is at least equal to $\lambda/3$ [36]. This latter condition implies that the receiver is no longer electrically small when

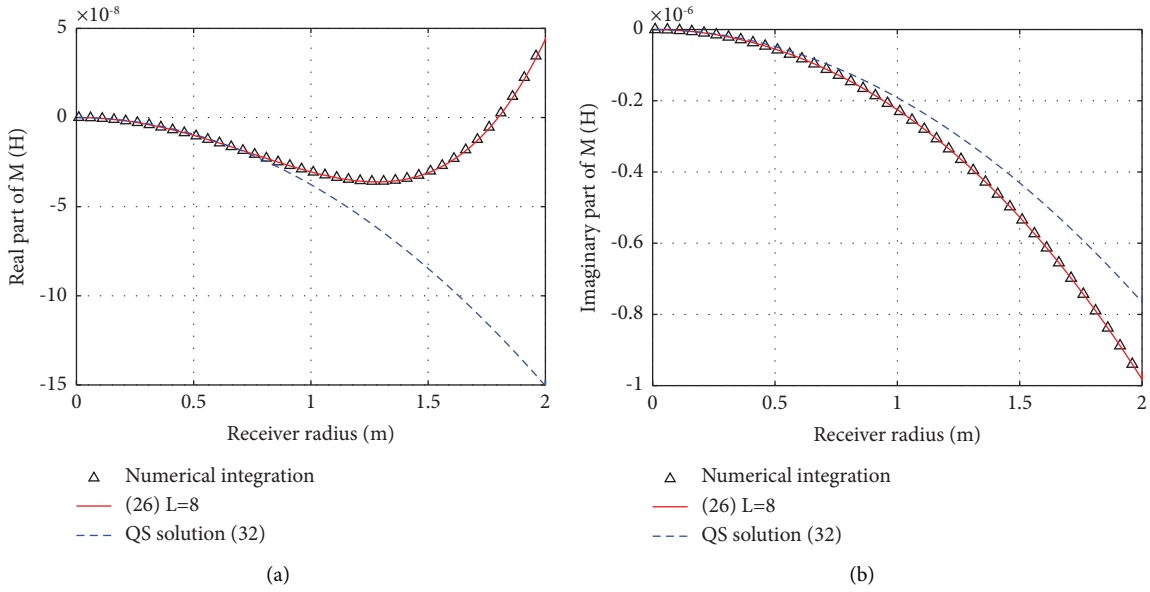

FIGURE 4: Flux linkage between two coils on a conducting soil plotted against the receiver radius b. (a) Real part of the flux linkage vs. b. (b) Imaginary part of the flux linkage vs. b.

$$b \geq \frac{\lambda}{6\pi} \cong 1.6\,m, \tag{35}$$

while it ceases to be physically small for smaller values of b, that is, when b becomes larger than $a/10 = 50$ cm. As shown by the curves plotted in Figure 4, the 50-cm limit is approximately where the trends for the real and imaginary parts of M arising from (32) start to deviate from the exact data.

The curves of Figure 4 also allow to conclude that at intermediate or high frequencies, the real and the imaginary parts of the flux linkage have different behaviors with increasing b. In particular, while the imaginary part is always negative in sign and monotonically decreases (i.e., increases in absolute value), the real part of M does the same only if the radius of the receiver is sufficiently small with respect to that of the emitter. When this is no longer true, the slope of the curve starts to diminish in absolute value as b is increased, with the result that the real part of M soon reaches its minimum value. Thereinafter, the real part starts to increase and, after zero-crossing, becomes positive in sign.

Finally, one would ask to what extent changing the soil properties affects the magnetic coupling between concentric coils. This point is clarified by Figure 5, which depicts b–profiles of the amplitude of the mutual inductance of two single-turn coils, with the ground conductivity σ taken as a parameter. The calculation has been performed by using (26), and the index at which the infinite sum is truncated is taken to be $L = 9$. The source loop, with radius $a = 20$ m, is assumed to operate at the frequency of 10 MHz, and three different values for σ are considered, while the relative dielectric permittivity of the ground is still assumed to be equal to 10. The obtained trends are compared to that arising from neglecting the presence of the ground, which comes from applying the well-known analytical expression [26]

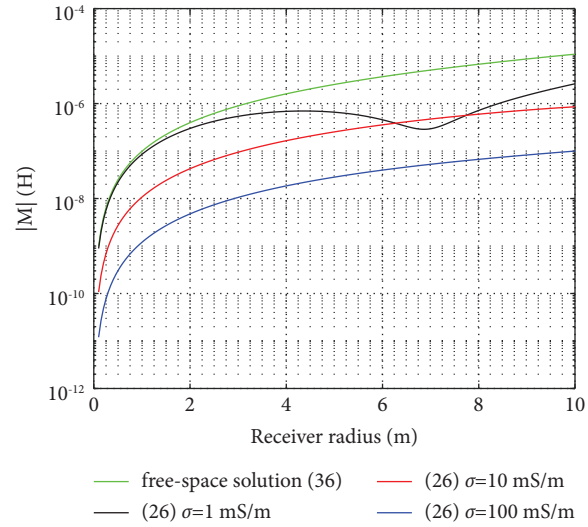

FIGURE 5: Magnitude of the mutual inductance of two coils placed on a conducting soil plotted against the receiver radius with the soil conductivity taken as a parameter.

$$M_{\text{free-space}} = \mu_0 \sqrt{ab}\left[\left(\frac{2}{\kappa} - \kappa\right)K(\kappa) - \frac{2}{\kappa}E(\kappa)\right], \tag{36}$$

where

$$\kappa = \frac{2\sqrt{ab}}{a+b}, \tag{37}$$

and with $K(\kappa)$ and $E(\kappa)$ being the complete elliptic integrals of the first and second kind, respectively. The curves plotted in Figure 5 point out how increasing the conductivity of the medium leads to reduce the mutual inductance of the loops.

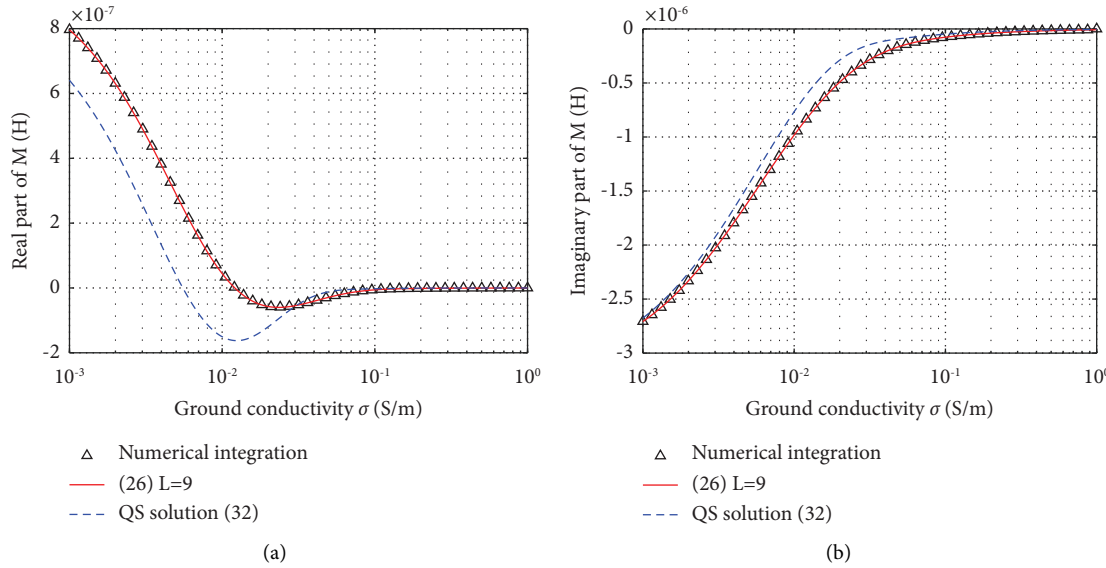

FIGURE 6: Flux linkage between two coils placed on a conducting soil plotted against the soil conductivity σ. (a) Real part of the flux linkage vs. σ. (b) Imaginary part of the flux linkage vs. σ.

This means that the amplitude of the mutual inductance reaches its maximum value when the two loops are embedded in free space.

The effect of changing the ground conductivity on the real and imaginary parts of the mutual inductance is illustrated by Figure 6. In this example, it is assumed that $a = 5$ m and $b = 2$ m, and the operating frequency is still taken to be equal to 10 MHz. The ground is characterized by relative dielectric permittivity equal to 10, while the electrical conductivity σ is comprised between 1 mS/m and 1 S/m. Again, the $\sigma-$ profiles of M arising from (26) and (32) and numerical integration of (6) are computed and plotted. From the analysis of the curves depicted in Figure 6, it is evident that at the frequency of 10 MHz, the impact of changing σ on the magnetic coupling is not negligible up to about 100 mS/m. This is true for both the components of M. In particular, for $\sigma \leq 100$ mS/m, the real part may assume positive as well as negative values, and its absolute value decreases almost everywhere as σ is increased. Conversely, the imaginary part of M is negative in sign all over the considered range of σ, and its absolute value monotonically decreases as σ grows up.

4. Conclusions

The purpose of the present work has been to derive an exact explicit analytical solution describing the flux linkage between two concentric coils positioned on a conducting terrestrial area. The solution has been derived through a purely analytical approach based on converting the complete single-integral expression for the flux linkage into a double integral consisting of a finite and a semi-infinite integral. Then, the semi-infinite integral is recognized to be a well-known tabulated Sommerfeld integral, which may be evaluated straightforwardly. Finally, Lommel's expansion is applied to convert the remaining finite integral into a combination of simpler integrals amenable to analytical evaluation. As a result, the flux linkage between the two coils is given as a sum of spherical Hankel functions of the wavenumber in the air and in the ground, multiplied by a coefficient depending on the geometrical dimensions of the coils. Numerical tests have been performed to test the validity of the proposed expression. It has been shown that with accuracy being equal, the time cost of the proposed approach is significantly smaller than that implied by numerical integration schemes.

Data Availability

The data used to support the findings of this study are available from the corresponding author upon reasonable request.

Conflicts of Interest

The author declares that there are no conflicts of interest.

References

[1] A. Stephan and K.-M. Strack, "A simple approach to improve the S/N ratio for TEM data using multiple receivers," *Geophysics*, vol. 56, no. 6, pp. 863–869, 1991.

[2] B. R. Spies and F. C. Frischknecht, "Electromagnetic sounding," in *Electromagnetic Methods in Applied Geophysics*, M. N. Nabighian, Ed., pp. 285–426, Society of Exploration Geophysicists, Houston, TX, USA, 1991.

[3] D. Kwiat, S. Saoub, and S. Einav, "Calculation of the mutual induction between coplanar circular surface coils in magnetic resonance imaging," *IEEE Transactions on Biomedical Engineering*, vol. 39, no. 5, pp. 433–436, 1992.

[4] P. Angelidis, K. Vassiliadis, and G. D. Sergiadis, "Lowest mutual coupling between closely spaced loop antennas," *IEEE Transactions on Antennas and Propagation*, vol. 39, no. 7, pp. 949–953, 1991.

[5] A. Kumar and P. A. Bottomley, "Optimized quadrature surface coil designs," *Magnetic Resonance Materials in Physics, Biology and Medicine*, vol. 21, no. 1-2, pp. 41–52, 2008.
[6] P. J. Gething, *Radio Direction Finding and Superresolution*, IET, London, UK, 1991.
[7] Y. T. Lo and S. Lee, *Antenna Handbook: Theory, Applications, and Design*, Springer Science & Business Media, New York, NY, USA, 2013.
[8] S. Lee, *Antenna Handbook: Volume III Applications*, Springer Science & Business Media, New York, NY, USA, 1993.
[9] C. A. Balanis, *Antenna Theory: Analysis and Design*, John Wiley & Sons, Hoboken, NJ, USA, 2012.
[10] A. W. Guy, J. F. Lehmann, and J. B. Stonebridge, "Therapeutic applications of electromagnetic power," *Proceedings of the IEEE*, vol. 62, no. 1, pp. 55–75, 1974.
[11] D. Schieber, "Some remarks on inductive and capacitive diathermy," *Journal of the Franklin Institute*, vol. 327, no. 4, pp. 515–526, 1990.
[12] A. Trivino-Cabrera, J. Aguado, and J. M. Gonzalez, "Analytical characterisation of magnetic field generated by icpt wireless charger," *Electronics Letters*, vol. 53, no. 13, pp. 871–873, 2017.
[13] T. Imura, H. Okabe, and Y. Hori, "Basic experimental study on helical antennas of wireless power transfer for electric vehicles by using magnetic resonant couplings," in *Proceedings of the 2009 IEEE Vehicle Power and Propulsion Conference*, pp. 936–940, Dearborn, MI, USA, September 2009.
[14] Y. Jang and M. M. Jovanovic, "A contactless electrical energy transmission system for portable-telephone battery chargers," *IEEE Transactions on Industrial Electronics*, vol. 50, no. 3, pp. 520–527, 2003.
[15] C. Xiao, D. Cheng, and K. Wei, "An lcc-c compensated wireless charging system for implantable cardiac pacemakers: theory, experiment, and safety evaluation," *IEEE Transactions on Power Electronics*, vol. 33, no. 6, pp. 4894–4905, 2018.
[16] L. Jianyu, T. Houjun, and G. Xin, "Frequency splitting analysis of wireless power transfer system based on t-type transformer model," *Electronics and Electrical Engineering*, vol. 19, no. 10, pp. 109–113, 2013.
[17] Y. Chung, T. Lee, and S. Y. Lee, "Characteristic comparison of different resonators to extend transfer distance in superconducting wireless power transfer for electric vehicle using high temperature superconducting resonance coil," *Journal of International Council on Electrical Engineering*, vol. 7, no. 1, pp. 249–254, 2017.
[18] Z. H. Shi, X. Y. Chen, and Z. C. Qiu, "Modeling of mutual inductance between superconducting pancake coils used in wireless power transfer (wpt) systems," *IEEE Transactions on Applied Superconductivity*, vol. 29, no. 2, pp. 1–4, 2019.
[19] Z. Zhang, K. Chau, C. Liu, F. Li, and T. Ching, "Quantitative analysis of mutual inductance for optimal wireless power transfer via magnetic resonant coupling," *IEEE Transactions on Magnetics*, vol. 50, no. 11, pp. 1–4, 2014.
[20] X. Zhang, H. Meng, B. Wei, S. Wang, and Q. Yang, "Mutual inductance calculation for coils with misalignment in wireless power transfer," *Journal of Engineering*, vol. 2019, no. 16, pp. 1041–1044, 2019.
[21] W. Dehui, S. Qisheng, W. Xiaohong, and Y. Fan, "Analytical model of mutual coupling between rectangular spiral coils with lateral misalignment for wireless power applications," *IET Power Electronics*, vol. 11, no. 5, pp. 781–786, 2018.
[22] S. Liu, J. Su, J. Lai, J. Zhang, and H. Xu, "Precise modeling of mutual inductance for planar spiral coils in wireless power transfer and its application," *IEEE Transactions on Power Electronics*, vol. 36, no. 9, pp. 9876–9885, 2021.
[23] J. C. Maxwell, *A Treatise On Electricity And Magnetism*, Dover, Downers Grove, IL, USA, 1954.
[24] S. Butterworth, "LIII. *On the coefficients of mutual induction of eccentric coils*," *The London, Edinburgh and Dublin Philosophical Magazine and Journal of Science*, vol. 31, no. 185, pp. 443–454, 1916.
[25] C. Snow, *Formulas for Computing Capacitance and Inductance*, Bureau of Standards Circular, Washington, DC, USA, 1954.
[26] C. M. Zierhofer and E. S. Hochmair, "Geometric approach for coupling enhancement of magnetically coupled coils," *IEEE Transactions on Biomedical Engineering*, vol. 43, no. 7, pp. 708–714, 1996.
[27] M. Parise, G. Antonini, and D. Romano, "On the flux linkage between pancake coils in resonance-type wireless power transfer systems," *International Journal of Antennas and Propagation*, vol. 2020, Article ID 8630978, 6 pages, 2020.
[28] M. Parise, V. Tamburrelli, and G. Antonini, "Mutual impedance of thin-wire circular loops in near-surface applications," *IEEE Transactions on Electromagnetic Compatibility*, vol. 61, no. 2, pp. 558–563, 2019.
[29] S. H. Ward and G. W. Hohmann, "Electromagnetic theory for geophysical applications," in *Electromagnetic Methods in Applied Geophysics*, M. N. Nabighian, Ed., pp. 130–311, Society of Exploration Geophysicists, Houston, TX, USA, 1988.
[30] M. Parise, "On the voltage response of homogeneous earth models in central loop electromagnetic sounding," *International Journal of Antennas and Propagation*, vol. 2022, Article ID 8294000, 7 pages, 2022.
[31] I. S. Gradshteyn and I. M. Ryzhik, *Table of Integrals, Series, and Products*, Academic Press, New York, NY, USA, 2007.
[32] G. N. Watson, *A Treatise on the Theory of Bessel Functions, Ser. Cambridge Mathematical Library*, Cambridge University Press, Cambridge, UK, 1944.
[33] M. Abramowitz and I. A. Stegun, "Handbook of mathematical functions: with formulas, graphs, and mathematical tables," *Courier Corporation*, vol. 55, 1964.
[34] M. Parise, "Exact EM field excited by a short horizontal wire antenna lying on a conducting soil," *AEU-International Journal of Electronics and Communications*, vol. 70, no. 5, pp. 676–680, 2016.
[35] D. H. Werner, "An exact integration procedure for vector potentials of thin circular loop antennas," *IEEE Transactions on Antennas and Propagation*, vol. 44, no. 2, pp. 157–165, 1996.
[36] C. A. Balanis, *Antenna Theory: Analysis and Design*, John Wiley & Sons, New York, NY, USA, 4th edition, 2016.
[37] H. J. Visser, *Antenna Theory and Applications*, John Wiley & Sons, New York, NY, USA, 2012.
[38] D. Foster, "Loop antennas with uniform current," *Proceedings of the IRE*, vol. 32, no. 10, pp. 603–607, 1944.
[39] W. M. Telford, L. Geldart, and R. E. Sheriff, *Applied Geophysics*, Cambridge University Press, Cambridge, UK, 1990.